Pure Appl. Chem., Vol. 82, No. 6, pp. 1301–1315, 2010.
doi:10.1351/PAC-CON-09-11-02
© 2010 IUPAC, Publication date (Web): 4 May 2010

Experimental and modeling study of O and Cl atoms surface recombination reactions in O_2 and Cl_2 plasmas*

Luc Stafford[1,‡], Joydeep Guha[2,3], Rohit Khare[2], Stefano Mattei[1], Olivier Boudreault[1], Boris Clain[1], and Vincent M. Donnelly[2]

[1]Department of Physics, University of Montréal, Montréal, Québec, H3C 3J7, Canada; [2]Department of Chemical and Biomolecular Engineering, University of Houston, Houston, TX 77204, USA; [3]Lam Research Corporation, Fremont, CA 94538, USA

Abstract: In low-pressure plasmas commonly used in materials processing, plasma–wall interactions play a crucial role in the evolution of the plasma properties both over time and across large-area wafers. We have recently studied the heterogeneous recombination of O and Cl atoms on reactor walls in O_2 and Cl_2 plasmas through both experiments and modeling. The Langmuir–Hinshelwood (i.e., delayed) recombination was investigated using a "spinning-wall" technique in which a portion of the substrate surface is periodically exposed to an inductively coupled plasma and to a differentially pumped chamber where either Auger electron spectroscopy (AES) or line-of-sight mass spectrometry (MS) is used to detect surface and desorbing species. In this paper, a review of the various effects driving the O and Cl atoms recombination dynamics on anodized aluminum (AA) and stainless steel (SS) surfaces is presented. It is shown that recombination probabilities, γ, can vary following plasma exposure due to surface conditioning. In Cl_2 plasmas, γ was also found to depend on the Cl-to-Cl_2 number density ratio, a mechanism ascribed to a competition for adsorption sites between Cl and Cl_2. We have also determined the recombination rates of Cl atoms in Cl_2 high-density plasmas sustained by electromagnetic surface waves by comparing the measured degrees of dissociation of Cl_2 to those predicted by an isothermal fluid model. For a reactor with large SS and quartz surfaces exposed to the plasma, γ values and their dependence on the Cl-to-Cl_2 number density ratio were consistent with those obtained from the rotating substrate technique. Similar values were obtained for plasmas sustained in a quartz discharge tube. It is expected that for plasmas sustained in or adjacent to a silica tube or plate, the Cl atoms recombination coefficient becomes independent of chamber wall material due to reactor seasoning, producing a silicon-oxychloride layer.

Keywords: chlorine plasmas; fluid modeling; oxygen plasmas; plasma; recombination.

INTRODUCTION

Low-temperature plasmas operated in O- and Cl-containing gas mixtures are now routinely used in materials processing. Applications of O_2 plasmas include the surface activation and cleaning of polymers

*Paper based on a presentation at the 19th International Symposium on Plasma Chemistry (ISPC-19), 26–31 July 2009, Bochum, Germany. Other presentations are published in this issue, pp. 1189–1351.
‡Corresponding author

[1], ashing of organic materials [2], and anisotropic etching of Si [3]. Cl_2 plasmas are employed to etch Si [4], metals [5], and high-k dielectrics [6] in the semiconductor industry and emerging materials such as transparent conducting oxides [7], electro-optic oxides [8], ferroelectrics [9], and ferromagnetics [10] of interest for the fabrication of optoelectronic, photonic, and spintronic devices. An important parameter to control for these applications is the number density of O and Cl atoms [11,12]. Under low-pressure plasma conditions (i.e., <100 mTorr), these species are created by electron-impact dissociation of O_2 and Cl_2 and are essentially lost by surface recombination processes on reactor walls and substrate [13–15].

The heterogeneous recombination rates of O and Cl atoms have been studied by many workers on various surfaces using a wide variety of experimental techniques. However, most methods were either based on non-local and local atom concentration measurements (e.g., by optical emission spectroscopy) [16,17] or based on indirect data such as the substrate temperature increase due to the heat deposited by the exothermic surface reaction [18]. Studies with high- or ultra-high-vacuum neutral beams allow quantitative methods such as line-of-sight mass spectrometry (MS) or Auger electron spectroscopy (AES) to be used to provide sticking coefficients and product yield, surface coverage, and activation energies. However, these conditions do not simulate very well the conditions of materials processing where substrates are in a dynamic environment with high fluxes of reactants and simultaneous bombardment by positive ions, electrons, UV and VUV photons. As a result, the recombination coefficients determined from beam studies for a given atom on a given material often vary by orders of magnitude with respect to those obtained under dynamic plasma conditions. For example, Kota et al. [19] found recombination coefficients for Cl atoms at 300 K of 0.2 for anodized Al and 0.7 for stainless steel (SS) in a molecular beam experiment while the values for these materials determined in high-density Cl_2 plasma reactors are usually in the 0.01–0.04 range [20–22]. An important factor influencing the surface recombination rates and thus the materials processing rates is the so-called "conditioning" or "seasoning" of the surface following exposure to reactive plasmas [23–26]. For example, Kim and Aydil [27] investigated the consequences of reactor seasoning on the rate and uniformity of Si etching in an inductively coupled Cl_2 plasma. The maximum etch rate shifted from the center of the wafer in an unseasoned reactor to the edge of the wafer when the walls were fully passivated, in this case with a $SiOCl_x$ film.

A "spinning-wall" technique was recently developed for studying surface reactions on plasma reactor walls [28–37]. This method couples the established ultra-high-vacuum techniques of desorption MS and AES to the high-pressure, high-charge-density plasma environment. A small, cylindrical substrate is rapidly rotated through skimmers such that a point of the surface is periodically exposed to the plasma and is analyzed in near real-time by surface diagnostics in separate, differentially pumped chambers. This paper reviews and compares previously published spinning-wall studies of the recombination dynamics of O and Cl atoms on plasma-conditioned AA and SS surfaces [28–35]. Cl atom recombination rate was also obtained by fitting an isothermal fluid model to measured degrees of dissociation of Cl_2 obtained in low-pressure, high-density Cl_2 plasmas sustained by traveling electromagnetic surface waves.

DESCRIPTION OF THE SPINNING-WALL APPARATUS

A schematic of the spinning-substrate apparatus used in this work is shown in Fig. 1. An inductively coupled plasma (ICP) operating at 13.56 MHz is ignited in a fused silica discharge tube and then expands into a processing chamber with AA walls. The lower end of the ICP source is surrounded by an electromagnet to confine the plasma in the downstream region. Experiments were performed in O_2 and Cl_2 plasmas for pressures in the 1.25–20 mTorr range and ICP powers between 100 and 600 W. The pressure was varied by adjusting a throttle valve located at the entrance of the pumping system. Langmuir probe and optical emission spectroscopy investigations of this plasma in O_2, Cl_2, and Cl_2/O_2 mixtures were presented in previous publications [28,31,36].

© 2010, IUPAC

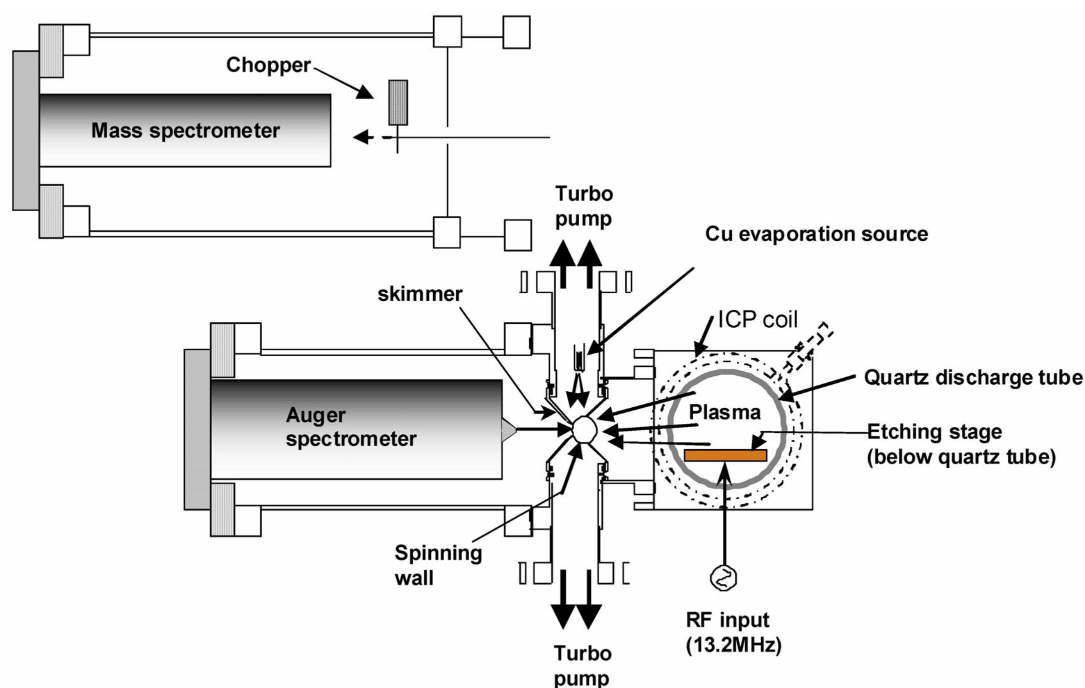

Fig. 1 Schematics of the spinning-wall apparatus, including an ICP reactor, and differentially pumped chamber containing either an AES or a line-of-sight, chopped MS, as shown in the expanded views (left). The plasma and intermediate chambers are separated by skimmers for differential pumping. The schematic also shows the evaporation source for Cu deposition and the Si etching stage.

The cylindrical substrate made of or coated with the material of interest is located in the first differentially pumped "substrate chamber" between the plasma chamber and an ultra-high-vacuum diagnostic chamber. In this work, two types of substrates were used: AA and electropolished SS (304L). Both AA and SS substrates can be rotated at speeds up to 100000 rpm by a brushless motor with ceramic bearings (Koford). A conical skimmer and differential pumping reduce the pressure in the substrate chamber by a factor of a thousand relative to the pressure in the plasma chamber. A further three-orders-of-magnitude pressure reduction is achieved in a second differentially pumped chamber with a similar conical skimmer. This chamber can house either an AES (Staib Instruments, DESA 150) for measurements of the surface composition or a third differentially pumped chamber with an MS (Extrel, 0–400 amu) for measurements of products desorbing from the substrate. For MS investigations, a 100 Hz tuning fork chopper was used to extract the line-of-sight component (chopper-open minus chopper-close) from the measured line-of-sight plus background signals [28].

In some experiments, a separately radio frequency (RF)-biased (13.2 MHz), water-cooled electrode with a thermally bonded Si wafer was installed in the processing chamber below the ICP source region [35]. This powered electrode was used to deposit Si on the spinning substrate (and chamber walls) while it is being rotated and analyzed by AES. To study the effect of trace amounts of metallic species on the recombination dynamics, a custom thermal evaporation source was installed in the substrate chamber [35]. In this work, high-purity Cu wires (Sigma Aldrich, 99.999 %) were used as the deposition source. For all experiments, the temperature of the filament was set to 1235 K, producing a Cu impingement flux on the spinning substrate of about 4.7×10^{11} cm^{-2} s^{-1}.

© 2010, IUPAC

DETERMINATION OF RECOMBINATION COEFFICIENTS USING THE SPINNING-WALL TECHNIQUE

Recombination of O atoms on plasma-conditioned AA and SS

As illustrated in Fig. 2, points along the mid-circumference of the substrate surface repeatedly enter the plasma, and some reactive species (e.g., O atoms) adsorb. Surface recombination reaction then leads to the formation and desorption of reaction products (e.g., O_2). These products can be detected either by an increase of the line-of-sight MS signal [28,29] or through a pressure rise measured with an ultra-high-vacuum ionization gauge in the AES chamber [32]. The dominant reaction product measured by MS following exposure of the substrate to an O_2 plasma was O_2 at $m/z = 32$ [28]. An example of the increase of the line-of-sight MS signal of O_2 as a function of substrate rotation frequency, f, for a 5 mTorr, 600 W O_2 plasma is shown in Fig. 3. The AES pressure rise obtained under comparable conditions for AA and SS surfaces are also shown for comparison. For AA, the O_2 MS signal and the AES pressure rise are seen to increase similarly with f, indicating that the pressure rise in the Auger chamber is a good indicator of the desorption flux of O_2 molecules following heterogeneous recombination of O atoms. At all substrate rotation frequencies, the pressure rises are higher for SS than for AA; we will come back on this point later on. One should note that when the substrate was spun with the plasma off, no increase was observed with rpm for both AA and SS substrates [28,34]. This indicates that, in our experimental conditions, O_2 (unlike Cl_2) [31,34] does not stick to the surface and therefore does not participate in the recombination reaction.

As discussed previously [28,31] and illustrated in Fig. 2, the experiments described above only detect Langmuir–Hinshelwood (LH) recombination reactions. In this case, O atoms adsorbed in a weakly bound (or physisorbed) state can diffuse on the surface before recombining with a more strongly bound (or chemisorbed) O atoms, allowing a substantial time between O adsorption and O_2 desorption. On the other hand, prompt Eley–Rideal (ER) recombination reactions between a gaseous atom and an adsorbed atom occur, if at all, during plasma exposure and are therefore not detected by MS or through a pressure rise in the Auger chamber. Based on the work of Kim and Boudart [38], Kota et al. [39], and

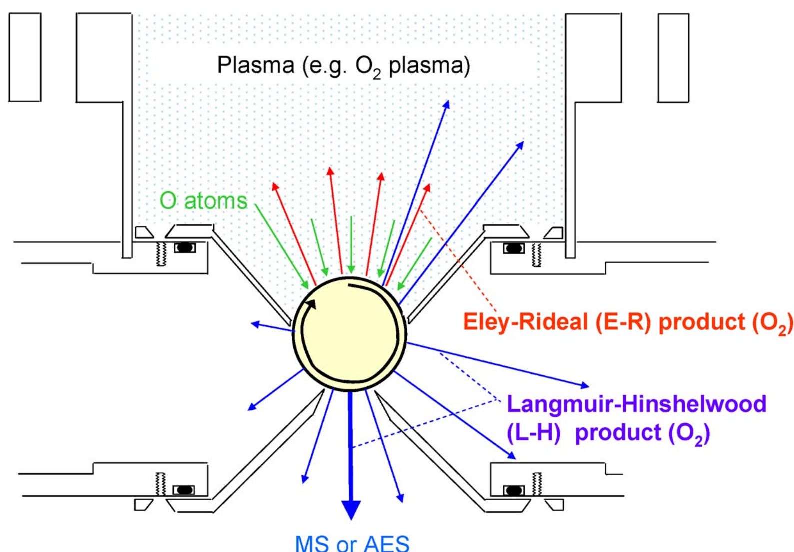

Fig. 2 Schematic of the O adsorption and O_2 desorption following ER and LH recombination reactions. Prompt ER reactions occur, if at all, during plasma exposure and are therefore not detected by MS or through a pressure rise in the Auger chamber.

© 2010, IUPAC

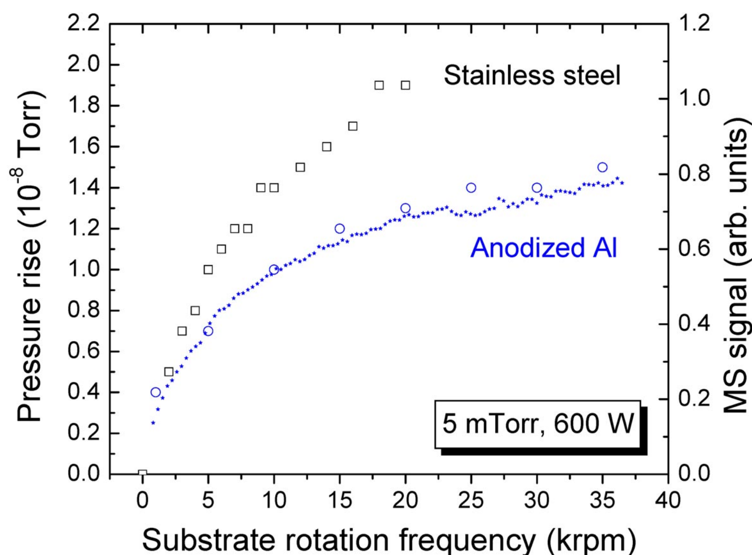

Fig. 3 Example of increase in the line-of-sight MS signal (filled symbol) and pressure rises in the Auger chamber (open symbols) as a function of substrate rotation frequency for AA and SS surfaces following their exposition to a 5 mTorr, 600 W O_2 plasma. The MS signals were scaled to match the pressure rise scale.

Guerra [40], one can nonetheless reasonably expect LH to dominate over ER for the sample temperature investigated here (~310 K as measured through a ZnSe window with a pyrometer) [28].

To extract surface reaction kinetics, the rotation-frequency-dependent MS signals and Auger pressure rises due to LH recombination presented in Fig. 3 were converted into absolute desorption fluxes, D^{rec}, using a calibration technique described elsewhere [31,32,34]. D^{rec} values vs. reaction time, t_r, are shown in Fig. 4 for AA and SS substrates. The reaction time is defined as the time taken for a point on the surface to rotate from the midpoint of plasma exposure to the midpoint of the region probed by MS and AES, i.e., $t_r = (2f)^{-1}$. The shortest t_r was 0.8 ms, corresponding to a rotation speed of 35 000 rpm. For comparison, we have also plotted the D^{rec} values for a silicon oxide surface sputter-deposited on top of an Al substrate. Details on the experimental conditions for sputter-deposition can be found in ref. [35]. Since the results for AA and SS were obtained in different plasma conditions than those for SiO_x, and thus involved different O impingement fluxes, Γ_O, ($\Gamma_O = 5.8 \times 10^{16}$ cm^{-2} s^{-1} for AA and SS [28]; $\Gamma_O = 5.1 \times 10^{16}$ cm^{-2} s^{-1} for SiO_x [35]), D^{rec} values were normalized by Γ_O. All curves presented in Fig. 4 show a non-exponential decay with increasing t_r. It was previously shown that this non-exponential behavior results from a mechanism in which O atoms recombine at differing rate on the surface at a distribution of sites [28,29,31]. The fast rate of recombination and desorption at short times indicates that a majority of surface sites are relatively efficient in recombining O, while the long tail is a result of the presence of a smaller fraction of sites where recombination is slower. Figure 4 further shows that despite the expected difference in the chemical and structural properties of each material in the near-surface region (AA surfaces are rough while electropolished SS surfaces are smooth) [34], all materials are characterized by a similar decrease of D^{rec}/Γ_O with increasing t_r, suggesting a similar distribution of binding energy sites.

The LH recombination coefficient of O atoms was determined by extrapolating the D^{rec}/Γ_O values displayed in Fig. 4 to $t_r \to 0$ to obtain the desorption flux at pseudo-steady-state condition, $D^{rec}_{t_r \to 0}$, where the rotation frequency is much faster than the rate-limiting step in O recombination and desorption [31]. In such conditions, it is as though the sample is continuously in the plasma and the O_2 desorption flux becomes independent of reaction time. LH recombination coefficients were then deter-

© 2010, IUPAC

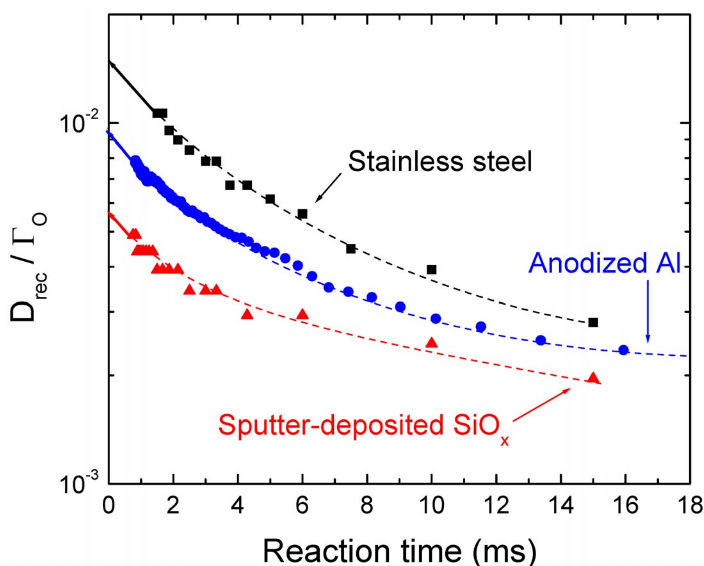

Fig. 4 Desorption flux, D^{rec}, derived from the data in Fig. 3, for O_2 formed by O atom recombination as a function of t_r (reciprocal of twice the rotation frequency) while the surface was exposed to a 5 mTorr, 600 W O_2 plasma. Plot of D^{rec} vs. t_r for a sputtered silica surface exposed to a 1.5 mTorr, 400 W O_2 plasma are also shown for comparison. For clarity, D^{rec} values were normalized to the O atom impingement flux, Γ_O.

mined from the relationship $\gamma_O = 6D^{rec}_{t_r \to 0}/\Gamma_O$, where the factor of 6 arises from the fact that there are 2 O atoms per O_2 molecules, divided by 1/3, the fraction of time that a point on the surface of the spinning substrate is exposed to the plasma per rotation.

Plots of D^{rec} vs. t_r were measured and the recombination coefficients were determined using the above analysis for a wide range of plasma conditions (1.25–20 mTorr, 100–600 W) and thus for a wide range of O impingement fluxes. These results were reported in previous publications [32,33], only the highlights are recalled here. For SS, Fig. 5 shows that γ_O was 0.09 ± 0.01 and was independent of Γ_O, indicating that the recombination reaction is first-order. Similar first-order behaviors for O atoms recombination were observed on pyrex, silica [41], and metal oxide surfaces (Cr_2O_3, Mn_2O_3, Fe_2O_3, Co_3O_4, NiO, Cu_2O, CuO, ZnO, CdO, and MgO) [42]. In the case of AA, recombination coefficients varied from $\gamma_O = 0.06 \pm 0.02$ in the limit of low O flux ($\Gamma_O \leq 1 \times 10^{16}$ cm^{-2} s^{-1}) to $\gamma_O = 0.04 \pm^{0.02}_{0.01}$ at $\Gamma_O = 7.5 \times 10^{16}$ cm^{-2} s^{-1}. These values are comparable to the $\gamma_O = 0.04 \pm 0.01$ value found on a sputtered silica surface [33].

The recombination probabilities for SS and AA displayed in Fig. 5 are much lower than those obtained in plasma chambers exclusively made of AA or SS, but similar to values recorded in systems with large silica surfaces exposed to the plasma. For example, Booth and Sadeghi [16] found $\gamma_O = 0.5$ in an electron cyclotron resonance plasma with SS walls. Similar values ($\gamma_O \sim 0.4$–0.6) were obtained for SS by Hsu et al. [43] in an ICP reactor with a Faraday shield to prevent erosion of the dielectric window due to capacitive coupling with the coil. The values found by the same group of authors were much lower and comparable to the ones determined from the spinning-wall technique when the Faraday shield was not present ($\gamma_O \sim 0.1$) [44,45]. Similar values for SS were found by Mozetic and Zalar [46] ($\gamma_O = 0.07$) in a cylindrical ICP sustained in a glass discharge tube and Matsushita et al. [47] ($\gamma_O = 0.1$) in the downstream region of a helicon plasma. The observation of low recombination coefficients on plasma-conditioned AA and SS surfaces with respect to those obtained on “bare” SS and AA result from the coating of sputtered silica on chamber walls due to the erosion of the silica discharge tube and viewports and the much lower γ_O values on SiO_x surfaces (e.g., $\gamma_O = 0.04$ for sputtered silica, see Fig. 5)

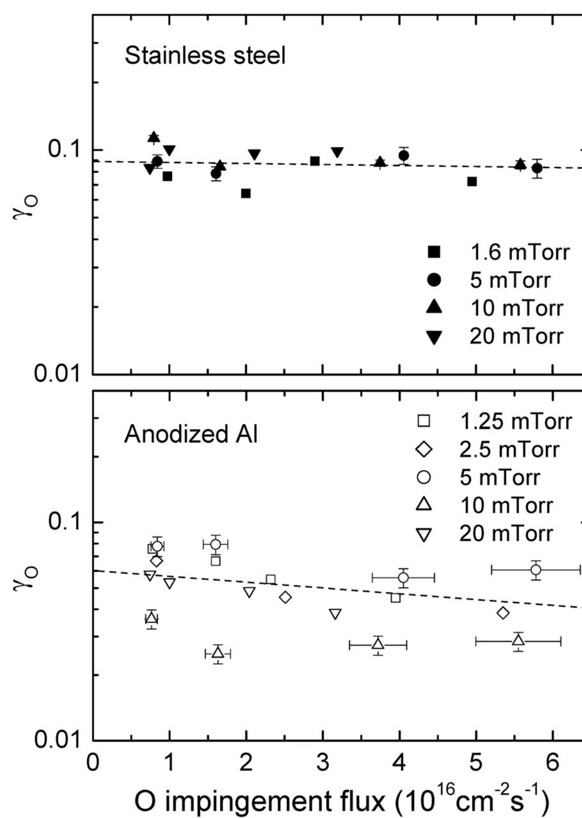

Fig. 5 Recombination coefficient of O atoms on plasma-conditioned SS (top) and AA (bottom) surfaces as a function of O flux varied by changing the plasma pressure and ICP power (adapted from refs. [32,33]).

[33]. Near real-time elemental analysis by in situ AES confirmed that the SS and AA surfaces became rapidly coated with a Si-oxide-based layer (Fe:Al:Si:O ≈ 1:1:3:8 for SS and Al:Si:O ≈ 2:1:3 for AA) [30,32]. The absolute concentration of Si determined by AES was comparable for SS (20 %) and AA (17 %) substrates, suggesting that the higher Auger pressure rises and thus the higher recombination coefficients for SS result from the presence of Fe on the surface. We will come back to this point.

Besides the erosion of the quartz discharge tube and viewports, other important contaminants for recombination reactions on chamber walls are the materials being processed [48,49]. For example, it has been found that the photoresist etching rate in a capacitively coupled O_2-based plasma decreases after the reactor has been exposed to Cu-containing wafers [50]. Also, the local photoresist etching rate in this reactor was depressed opposite to a Cu coupon attached to the upper electrode [50,51]. In ref. [33], we examined the effect of Cu contamination on the recombination dynamics of O atoms. To this end, trace amounts of Cu were deposited on the SiO_x surface using an in situ thermal evaporation source located in the first differentially pumped chamber (see Fig. 1). As in Figs. 3 and 4, the recombination coefficient was determined by measuring the pressure rise in the Auger chamber as a function of reaction time probed by changing the substrate rotation frequency and by extrapolating D^{rec} to $t_r \rightarrow 0$. The highlights of this study are presented in Fig. 6 where γ_O values are shown as a function of total Cu dose varied by increasing the exposure time to the evaporation source for a given filament temperature. Deposition of a small fraction of a monolayer (1 ml = 1.8×10^{15} cm^{-2} for SiO_2) produced an increase of 60 % of γ_O (γ_O = 0.07) over the Cu-free surface (γ_O = 0.04). With the first few doses, Cu was not detected on the surface, as it was below the detection limit of our Auger spectrometer (0.1 ml). Much

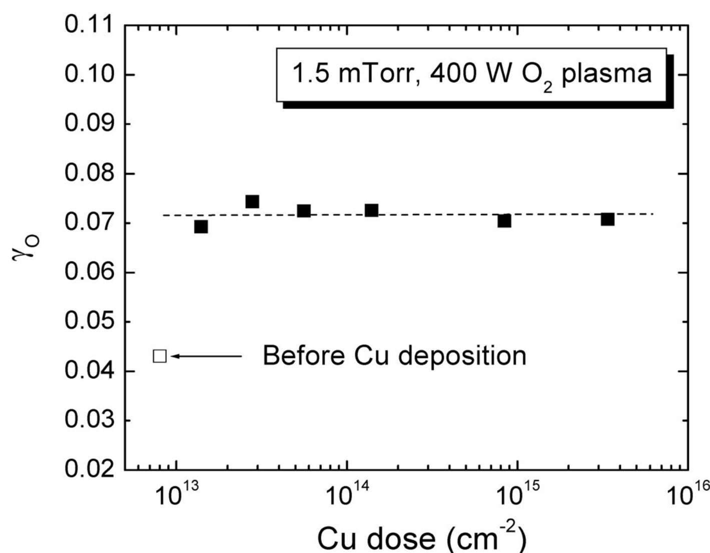

Fig. 6 Recombination coefficients of O atoms on oxidized Si measured before and after successive Cu doses of 1.4×10^{13}, 2.8×10^{13}, 5.6×10^{13}, 1.4×10^{14}, 8.4×10^{14}, and 3.4×10^{15} cm^{-2} (adapted from ref. [35]).

larger doses (up to 4×10^{15} cm^{-2}) resulted in detectable Cu (0.8 atom %, averaged over a ~3 nm depth probed by AES) but produced no further increase of γ_O. These results indicate that Cu catalyzes the recombination of O atoms in a LH reaction. The catalytic action of Cu is well known and is believed to result from its ability to change between the +1 and +2 oxidation states [52–55]. Fe is known to behave similarly, cycling between Fe^{2+} and Fe^{3+} [56]. This suggests that the higher recombination coefficients displayed in Fig. 4 for SS coated with sputtered silica with respect to those obtained on pure sputtered silica results from the presence of Fe on the surface playing a catalytic role similar to that of Cu.

Recombination of Cl atoms on plasma-conditioned AA and SS

Following the experiments in the O_2 plasma, the SS and AA substrates were exposed to a Cl_2 plasma for several hours and then analyzed by AES. As reported by several authors (see, e.g., refs. [57,58]), the surface became coated with a Si-oxychloride-based layer (Fe:Si:O:Cl ≈ 1:13:13:3 for SS and Al:Si:O:Cl ≈ 3:3:8:1 for AA) [30,34] due to Cl adsorption and the erosion of the silica discharge tube. In the case of AA, previous AES investigations indicated that the steady-state surface composition when going from a pure O_2 to pure Cl_2 plasma is reached in less than 300 s [37]. The absolute concentration of Si on the SS surface (45 %) was higher than on AA (22 %). The concentration of Cl was also larger (8.4 vs. 6.6 %), suggesting that the Si and Cl impinging species have a larger sticking probability on SS than on AA, or that these species diffuse into the more porous anodized Al coating, where they become undetectable by AES.

As in the section above, analysis of the products desorbing from these plasma-conditioned surfaces was performed through measurements of the increase of the line-of-sight MS signal [32] or through a pressure rise in the AES chamber [34]. The only desorption product measured by MS was Cl_2 (i.e., no Cl, $AlCl_x$, or $SiCl_x$ desorb) [31]. An example of pressure rise vs. substrate rotation frequency is shown in Fig. 7 for the plasma-conditioned SS substrate for a 20 mTorr Cl_2 pressure with the plasma off and on (600 W). Unlike for O_2, a rotation-frequency-dependent pressure rise was observed for Cl_2 with the plasma on as well as off. Desorption of Cl_2 with the plasma off can be attributed to either the physisorption–desorption of Cl_2, or another mechanism involving dissociative adsorption of Cl_2 fol-

© 2010, IUPAC

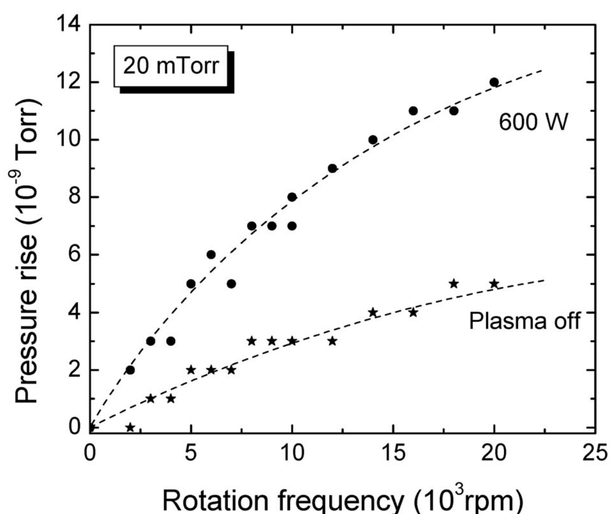

Fig. 7 Pressure rise measurements for a plasma-conditioned SS substrate for a 20 mTorr, 600 W Cl_2 plasma as a function of substrate rotation frequency. Pressure rises with the plasma off are also shown for comparison (taken from ref. [34]).

lowed by surface recombination of adsorbed Cl atoms and desorption of Cl_2. The approach to extract the portion of the pressure rise with the plasma on that is due to LH recombination of adsorbed Cl atoms, ΔP_{rec}, was described in details previously [30]. It was calculated according to $\Delta P_{rec} = \Delta P_{on} - (n^{on}_{Cl_2}/n^{off}_{Cl_2})\ \Delta P_{off}$, where ΔP_{on} and ΔP_{off} are the pressure rises with the plasma on and off, respectively. The net Cl_2 desorption due to Cl atoms recombination, D^{rec}, was then calculated using the same calibration procedure as for O atoms recombination. Finally, the recombination coefficient was obtained from the relationship $\gamma_{Cl} = 6D^{rec}_{t_r \to 0}/\Gamma_{Cl}$, where $D^{rec}_{t_r \to 0}$ is the net desorption due to LH recombination extrapolated to $t_r = 0$ and Γ_{Cl} is the Cl atoms impingement flux [31].

Plots of D^{rec} vs. t_r measured for a wide range of plasma conditions (1.25–20 mTorr, 100–600 W) were reported in refs. [31,34]. The recombination coefficients determined from these graphs using the above analysis are summarized in Fig. 8 as a function of the Cl/Cl_2 number density ratio. For SS, γ_{Cl} ranged from 0.004 to 0.03 and increased with Cl-to-Cl_2 number density ratio. A similar behavior was observed on plasma-conditioned AA; γ_{Cl} values reported are however larger by about a factor of 2. As expected, these values are much lower than those obtained by Kota et al. [19] for bare SS ($\gamma_{Cl} = 0.7$) and bare AA surfaces ($\gamma_{Cl} = 0.2$) due to the coating of sputtered silica on chamber walls and the much lower recombination coefficients of Cl atoms on silica-based surfaces ($\gamma_{Cl} < 0.005$) [39]. The lower values of γ_{Cl} on the plasma-conditioned SS surface can probably be attributed to the higher Si coverage (45 % for SS vs. 21.5 % for AA) and the smoother surface morphology [34].

The peculiar behavior of γ_{Cl} vs. Cl/Cl_2 number density ratio presented in Fig. 8 is in sharp contrast to the result obtained for O atoms recombination displayed in Fig. 5 where γ_O was found to be first-order with respect to the O impingement flux. Unlike O_2, a substantial amount of Cl_2 adsorption and desorption was observed with the plasma off [31,34]. Therefore, with the plasma on, Cl_2 adsorption can block sites for Cl adsorption and LH recombination. For a given Cl number density, γ_{Cl} thus decreases as the Cl_2 number density in the plasma increases. Over the range of experimental conditions investigated here (1.25–20 mTorr; 100–600 W), no competition for adsorption sites between O and O_2 was observed. It is possible, however, that this effect could begin to occur in plasmas with large concentrations of O_2 and much lower O/O_2 number density ratios. For example, Tserepi and Miller [59] found that γ_O decrease with O_2 pressure increasing from 100 mTorr to 3 Torr. In our case, the estimated O-to-O_2 number density ratios are in the 10^{-3}–10^{-1} range [28], which is similar to the ones estimated for the

© 2010, IUPAC

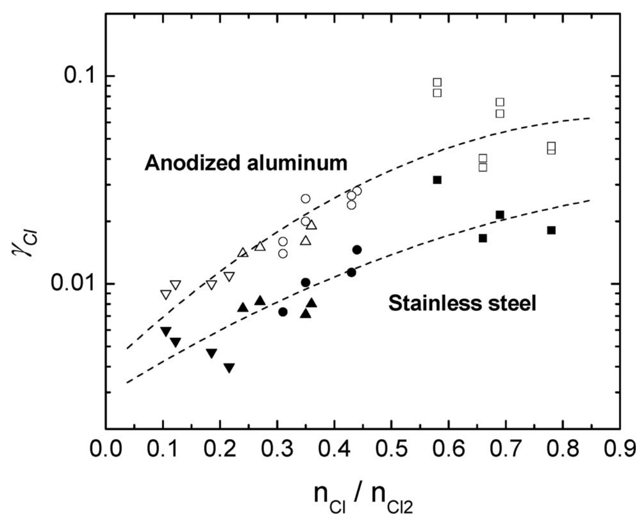

Fig. 8 Recombination coefficient of Cl atoms on plasma-conditioned SS (filled symbols) and plasma-conditioned anodized Al (open symbols) as a function of the Cl-to-Cl_2 number density ratio varied by changing the plasma pressure (1.25–20 mTorr) and ICP power (100–600 W). Inverted triangles, triangles, circles, and squares correspond to 20, 10, 5, and 1.25 mTorr pressures. Dashed lines are to guide the eye only (taken from refs. [31,34]).

conditions of Tserepi and Miller. This suggests that n_O/n_{O2} and n_{Cl}/n_{Cl2} are not the only parameters to consider; the absolute number densities of O_2 or Cl_2 impinging on the surface also play important roles in the recombination dynamics.

DETERMINATION OF THE RECOMBINATION PROBABILITY THROUGH MODELING

Recombination of Cl atoms in a large-volume high-density Cl_2 plasma reactor with large SS and silica surfaces exposed to the plasma

To further validate the recombination coefficients determined from the rotating substrate technique and its dependence on the plasma properties, we have compared the degree of dissociation measured in a high-density Cl plasma sustained by a 190 MHz electromagnetic surface wave to those predicted by an isothermal fluid model. Details on this plasma reactor, the model, and the recombination coefficients presented here can be found elsewhere [21,34,60]. The plasma is created in a 14.6-cm-diameter fused silica tube and expands from the source region into a large 28-cm-diameter SS processing chamber. Both in the source region and the downstream chamber, the plasma can be confined by the action of an axial magnetic field. Depending on gas pressure and magnetic field intensity, electron densities and temperatures in the downstream region of this reactor are in the 10^9–10^{11} cm^{-3} and 2–4 eV range, respectively. The gas temperature measured by plasma-sampling MS and determined from the $C^3\Pi_u$ $v = 0 \rightarrow B^3\Pi_g$ $v = 0$ emission rotational spectra of N_2 inserted as a tracer [61] was close to room temperature. The degree of dissociation of Cl_2 molecules determined by plasma-sampling MS [60] and actinometry on Cl_2 molecules using Xe as the actinometer gas and the zero-power extrapolation technique [62] are shown in Fig. 9 as a function of gas pressure.

These data were fitted to the predictions of a fluid model in which the particle balance equations for electrons, Cl, Cl_2, Cl^+, Cl_2^+, and Cl^- are solved together with the corresponding flux equations and the energy balance equations. The reaction set used was taken from Lee and Lieberman [15]. For simplicity, the plasma was assumed isothermal, which means that the electron temperature was considered as spatially uniform. This model was found to adequately predict the influence of gas pressure, mag-

© 2010, IUPAC

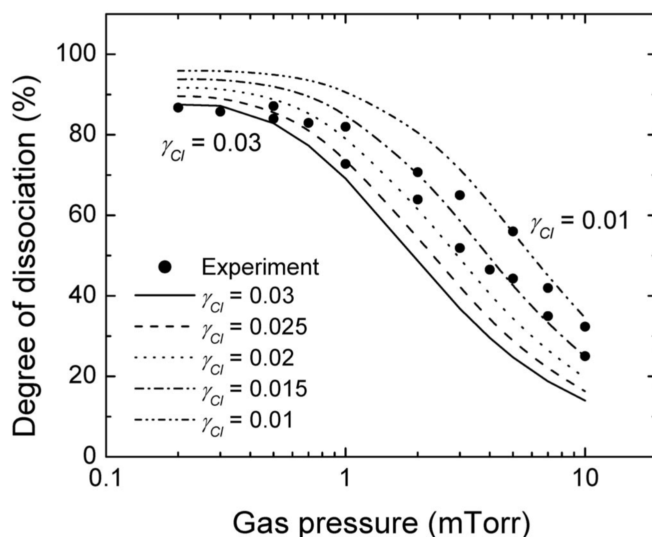

Fig. 9 Influence of gas pressure on the degree of Cl_2 dissociation in a Cl_2 high-density plasma sustained by traveling electromagnetic surface waves in an SS chamber with large amount of silica exposed to the plasma. Dashed lines are the predictions of a fluid model for different values of γ_{Cl} (taken from refs. [21,34]).

netic field intensity, and injected power on the electron number density, electron temperature, and number density of the dominant positive ion species [21]. As for the degree of dissociation of Cl_2, given that electron density and electron temperature are well computed, the only parameter that needs to be adjusted is the recombination coefficient of Cl atoms on chamber walls. Figure 9 shows the percent dissociation of Cl_2 predicted by the model for different values of γ_{Cl}. Over the wide range of pressures studied, none of the model curves seem to adequately fit the experimental data. As pressure increases, the value of γ_{Cl} needed to fit the measurement increases. This observation is consistent with the results obtained from the spinning-wall experiments displayed in Fig. 8. In addition, for comparable Cl-to-Cl_2 number density ratio, the absolute values of γ_{Cl} are also in good agreement. These values are also comparable to the ones obtained by Malyshev et al. [22] ($\gamma_{Cl} = 0.04$ for $n_{Cl}/n_{Cl_2} \sim 30$) and by Corr et al. [63] ($\gamma_{Cl} = 0.02$ for $n_{Cl}/n_{Cl_2} \sim 3$) in highly and moderately dissociated Cl_2 ICP and by Richard and Sawin [64] ($\gamma_{Cl} = 0.007$ for $n_{Cl}/n_{Cl_2} \sim 0.08$) in a weakly dissociated capacitively coupled plasma.

Recombination of Cl atoms in a small-volume, high-density Cl_2 plasma reactor sustained in quartz discharge tube

An approach similar to the one used in the section above was employed to extract the recombination coefficient of Cl atoms in a discharge tube. The plasma under investigation was produced in a 6-mm inside diameter fused silica tube by a propagating surface wave at 2.45 GHz [65,66]. The line-integrated electron density measured with phase-sensitive microwave interferometry [67], the percent dissociations of Cl_2 determined by actinometry on Cl_2 molecules using Xe as the actinometer [62] and the electron temperature, T_e, obtained by trace-rare-gas optical emission spectroscopy (TRG-OES) [68] are shown in Fig. 10 as a function of axial distance with respect to the wave launcher for a 50 mTorr, Cl_2 plasma. The absorbed (i.e., incident minus reflected) power was 60 W, producing a plasma approximately 15 cm long.

The measured line-integrated electron densities presented in Fig. 10a were used as inputs in the isothermal fluid model described in ref. [21]. For a given electron density (and thus for a given axial position), the Cl atom recombination coefficient was varied between 10^{-3} and 10^{-1} to match the meas-

© 2010, IUPAC

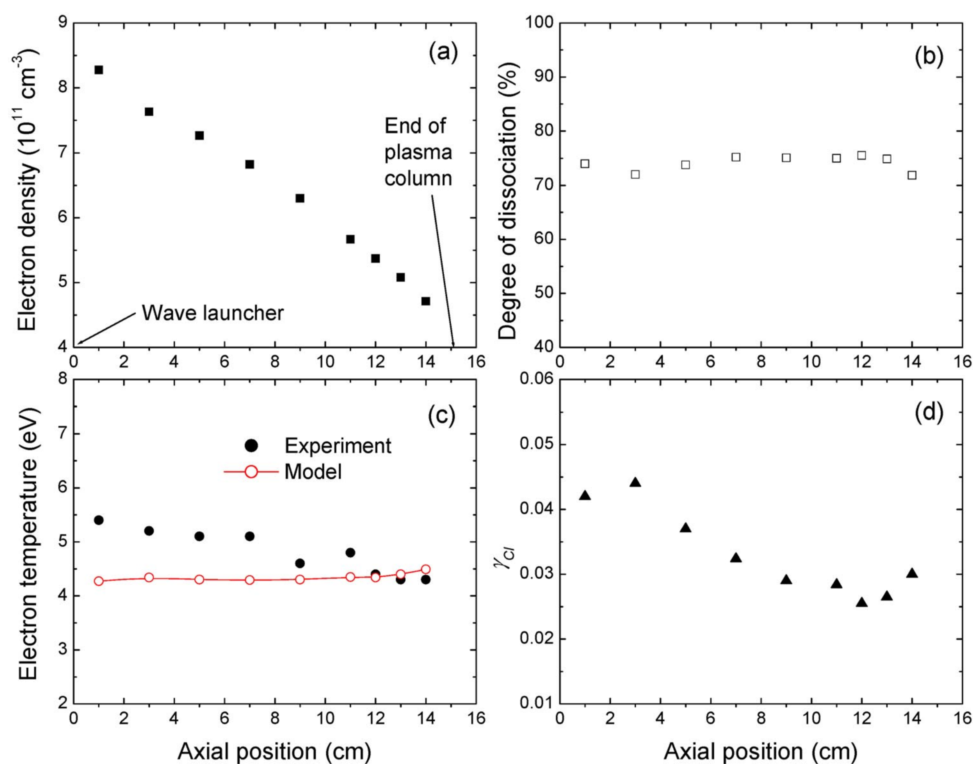

Fig. 10 Axial profile of the line-integrated electron density (a), Cl_2 percent dissociation (b), electron temperature (c), and Cl atoms recombination coefficient (d) for a 50 mTorr, Cl_2 plasma sustained by propagating electromagnetic surfaces in a quartz discharge tube. The T_e values predicted by the model are also shown for comparison.

ured percent dissociation of Cl_2 (Fig. 10b). The values of T_e and γ_{Cl} deduced from this fit are shown in Fig. 10 vs. axial distance. Considering that uncertainties on T_e determination from TRG-OES exceed 1 eV at high electron temperatures [68], T_e values deduced from the model are in very good agreement with measured values. In the range of experimental conditions investigated, γ_{Cl} ranges from 0.02–0.04. For example, at $z = 1$ cm, $\gamma_{Cl} \sim 0.042$ while at $z = 13$ cm, $\gamma_{Cl} \sim 0.026$. These values are much higher than those reported for a smooth, annealed quartz surface at 300 K after long exposure to a Cl atomic beam ($\gamma_{Cl} < 0.005$) [19,69] and are in fact closer to those found for AA and SS surfaces at high Cl-to-Cl_2 number density ratio (0.02–0.08, see Fig. 8). In those studies, AES analysis revealed that the spinning wall became coated with an SiO_xCl_y layer, due to erosion on the quartz discharge tube after operating the plasma for periods long enough to attain a "conditioned" steady-state surface. It is expected that the quartz tube used in the surface wave plasma study also eroded and roughened, therefore, the deposited SiO_xCl_y layer on the tube would be expected to behave like those in the spinning-wall studies and not as a smooth quartz surface. It is likely that the Cl recombination coefficient will be independent of chamber wall material in any type of plasma that is sustained in or adjacent to a silica tube or plate.

In Fig. 10, γ_{Cl} slightly decreases as we move away from the wave launcher. It is, however, a relatively small effect that could just be within the uncertainty of the experimental data and the fitting operation. It cannot be attributed to the dependence of γ_{Cl} on the Cl-to-Cl_2 number density ratio presented in Fig. 8 since the percent dissociation of Cl_2 was fairly constant axially (see Fig. 10b). It could be attributed to some temperature dependence of γ_{Cl}. An increase of γ with gas temperature was observed

by Wickramanayaka et al. [70] for the recombination of O atoms on pyrex in the downstream flow of an O_2 RF discharge. A similar result was found by Greaves and Linett [41]: γ_O increased from 1.6×10^{-4} at 20 °C to 1.4×10^{-2} at 600 °C. For a 50 mTorr, Cl_2 plasma, the gas temperature determined from the measured ro-vibrational emission spectra of N_2 inserted as a tracer [61] decreased with increasing axial distance, going from 612 ± 20 K near the wave launcher to 504 ± 20 K near the end of the plasma column. It is, however, difficult to estimate how T_g links to the actual wall temperature and thus to determine if the observed fall off of γ_{Cl} with distance results can be attributed to temperature effects.

CONCLUSION

In summary, we have observed the recombination of O and Cl atoms on dynamic SS and AA surfaces in inductively coupled O_2 and Cl_2 plasmas using the spinning-wall method. Overall, γ values were much lower than those expected for "bare" SS and AA surface due to the formation of a Si-oxide-based layer due to the slow erosion of the fused silica discharge tube. For O atoms recombination, we observed an increase of γ_O with the presence of Fe and Cu on the surface. These results were attributed to the strong catalytic activity of Fe and Cu due to their ability to change between two oxidation states. For both AA and SS surfaces, the recombination probability of Cl atoms was found to increase with the Cl-to-Cl_2 number density ratio, a result that can be ascribed to a competition for adsorption sites between Cl_2 and Cl. We have also determined the recombination rates of Cl atoms in Cl_2 high-density plasmas sustained by electromagnetic surface waves by comparing the measured degree of dissociation of Cl_2 to those predicted by an isothermal fluid model. For a reactor with large SS and quartz surfaces exposed to the plasma, γ values and their dependence with n_{Cl}/n_{Cl_2} were consistent with those obtained from the rotating substrate technique. Similar values were also obtained for plasmas sustained in a quartz discharge tube. It is likely that the Cl recombination coefficient will be independent of chamber wall material in any type of plasma that is sustained in or adjacent to a silica tube or plate.

ACKNOWLEDGMENTS

This research was supported by the National Science and Engineering Research Council (NSERC), the Fonds Québécois de la Recherche sur la Nature et les Technologies (FQRNT), the National Science Foundation (NSF), and Lam Research Corporation.

REFERENCES

1. F. Dreux, S. Marais, F. Poncin-Epaillard, M. Metayer, M. Labbé. *Langmuir* **18**, 10411 (2002).
2. D. A. Carl, D. W. Hess, M. A. Lieberman. *J. Appl. Phys.* **68**, 1859 (1990).
3. C. J. Mogab, A. C. Adams, D. L. Flamm. *J. Appl. Phys.* **49**, 3796 (1978).
4. S. Samukawa. *Appl. Phys. Lett.* **68**, 316 (1996).
5. R. Ramos, G. Cunge, O. Joubert, T. Lill. *J. Vac. Sci. Technol. B* **27**, 113 (2009).
6. L. Sha, J. P. Chang. *J. Vac. Sci. Technol. A* **22**, 88 (2004).
7. W. T. Lim, L. Stafford, J. I. Song, J. S. Park, Y. W. Heo, J. H. Lee, J. J. Kim, S. J. Pearton. *Appl. Surf. Sci.* **253**, 2752 (2006).
8. P.-M. Bérubé, J.-S. Poirier, J. Margot, L. Stafford, P. F. Ndione, M. Chaker, R. Morandotti. *J. Appl. Phys.* **106**, 063302 (2009).
9. L. Stafford, J. Margot, O. Langlois, M. Chaker. *J. Vac. Sci. Technol. A* **21**, 1247 (2003).
10. J. J. Wang, J. R. Childress, S. J. Pearton, F. Sharifi, K. H. Dahmen, E. S. Gillman, F. J. Cadieu, R. Rani, X. R. Qian, C. Li. *J. Electrochem. Soc.* **145**, 2512 (1998).
11. A. P. Mahorowala, H. H. Sawin. *J. Vac. Sci. Technol. B* **20**, 1077 (2002).
12. C. Lee, D. B. Graves, M. A. Lieberman. *Plasma Chem. Plasma Processing* **16**, 99 (1996).

© 2010, IUPAC

13. M. L. Brake, R. L. Kerber. *Plasma Chem. Plasma Processing* **3**, 79 (1983).
14. S. C. Deshmukh, D. J. Economou. *J. Appl. Phys*. **72**, 4597 (1992).
15. C. M. Lee, M. A. Lieberman. *J. Vac. Sci. Technol. A* **13**, 368 (1995).
16. J. P. Booth, N. Sadeghi. *J. Appl. Phys.* **70**, 611 (1991).
17. S. Gomez, P. G. Steen, W. G. Graham. *Appl. Phys. Lett.* **81**, 19 (2002).
18. M. Mozetic, A. Zalar. *Appl. Surf. Sci.* **158**, 263 (2000).
19. G. P. Kota, J. W. Coburn, D. B. Graves. *J. Vac. Sci. Technol. A* **16**, 270 (1998).
20. M. V. Malyshev, V. M. Donnelly, A. Kornblit, N. A. Ciampa. *J. Appl. Phys.* **84**, 137 (1998).
21. L. Stafford, J. Margot, F. Vidal, M. Chaker, K. Giroux, J. S. Poirier, A. Quintal-Léonard, J. Saussac. *J. Appl. Phys*. **98**, 063301 (2005).
22. M. V. Malyshev, V. M. Donnelly. *J. Appl. Phys*. **88**, 6207 (2000).
23. G. W. Lee, Y. B. Kang. *Electrochem. Solid State Lett.* **6**, G49 (2003).
24. K. Miwa, T. Mukai. *J. Vac. Sci. Technol. B* **20**, 2120 (2002).
25. G. Cunge, O. Joubert, N. Sadeghi. *J. Appl. Phys*. **94**, 6285 (2003).
26. A. Agarwal, M. J. Kushner. *J. Vac. Sci. Technol. A* **26**, 498 (2008).
27. T. W. Kim, E. S. Aydil. *J. Electrochem. Soc*. **150**, G418 (2003).
28. P. F. Kurunczi, J. Guha, V. M. Donnelly. *J. Phys. Chem. B* **109**, 20989 (2005).
29. P. F. Kurunczi, J. Guha, V. M. Donnelly. *Phys. Rev. Lett.* **96**, 018306-1 (2006).
30. J. Guha, Y.-K. Pu, V. M. Donnelly. *J. Vac. Sci. Technol. A* **25**, 347 (2006).
31. J. Guha, V. M. Donnelly, Y.-K. Pu. *J. Appl. Phys.* **103**, 013306 (2008).
32. L. Stafford, J. Guha, V. M. Donnelly. *J. Vac. Sci. Technol. A* **26**, 455 (2008).
33. J. Guha, P. Kurunczi, L. Stafford, V. M. Donnelly, Y.-K. Pu. *J. Phys. Chem. C* **112**, 8963 (2008).
34. L. Stafford, R. Khare, J. Guha, V. M. Donnelly, J.-S. Poirier, J. Margot. *J. Phys. D: Appl. Phys.* **42**, 055206 (2009).
35. J. Guha, R. Khare, L. Stafford, V. M. Donnelly, S. Sirard, E. A. Hudson. *J. Appl. Phys.* **105**, 113309 (2009).
36. J. Guha, V. M. Donnelly. *J. Appl. Phys*. **105**, 113307 (2009).
37. J. Guha, V. M. Donnelly. *J. Vac. Sci. Technol. A* **27**, 515 (2009).
38. Y. C. Kim, M. Boudart. *Langmuir* **7**, 2999 (1991).
39. G. P. Kota, J. W. Coburn, D. B. Graves. *J. Vac. Sci. Technol. A* **16**, 270 (1998).
40. V. Guerra. *IEEE Trans. Plasma Sci.* **35**, 1397 (2007).
41. J. C. Greaves, J. W. Linnett. *Trans. Faraday Soc.* **55**, 1346 (1959).
42. P. G. Dickens, M. B. Sutcliffe. *Trans. Faraday Soc.* **60**, 1272 (1964).
43. C.-C. Hsu, M. A. Nierode, J. W. Coburn, D. B. Graves. *J. Phys. D* **39**, 3272 (2006).
44. H. Singh, J. W. Coburn, D. B. Graves. *J. Appl. Phys.* **88**, 3748 (2000).
45. M. W. Kiehlbauch, D. B. Graves. *J. Vac. Sci. Technol. A* **21**, 660 (2003).
46. M. Mozetic, A. Zalar. *Appl. Surf. Sci.* **158**, 263 (2000).
47. J. Matsushita, K. Sasaki, K. Kadota. *Jpn. J. Appl. Phys.* **36**, Part 1, 4747 (1997).
48. G. Cunge, N. Sadeghi, R. Ramos. *J. Appl. Phys.* **102**, 093305 (2007).
49. S. Imai. *J. Vac. Sci. Technol. A* **27**, 1 (2009).
50. E. A. Hudson, S. Sirard. Unpublished.
51. G. Delgadino, D. Keil, J. Booth, C. Lee. *Proceedings of the Dry Process International Symposium*, Vol. 13 (unpublished) (2007).
52. J. Valyon, W. K. Hall. *J. Phys. Chem*. **97**, 7054 (1993).
53. M. Iwamoto, H. Yahiro, K. Tanda, N. Mizuno, Y. Mine, S. Kagawa. *J. Phys. Chem*. **95**, 3727 (1991).
54. D.-J. Liu, H. J. Robota. *Catal. Lett.* **21**, 291 (1993).
55. J. Valyon, W. S. Millman, W. K. Hall. *Catal. Lett.* **24**, 215 (1994).
56. J. O. Petunchi, W. K. Hall. *J. Catal.* **78**, 327 (1982).

© 2010, IUPAC

57. S. J. Ullal, A. R. Godfrey, E. Edelberg, L. Braly, V. Vahedi, E. S. Aydil. *J. Vac. Sci. Technol. A* **20**, 43 (2002).
58. S. J. Ullal, H. Singh, V. Vahedi, E. S. Aydil. *J. Vac. Sci. Technol. A* **20**, 499 (2002).
59. A. D. Tserepi, T. A. Miller. *J. Appl. Phys*. **77**, 505 (1995).
60. L. Stafford, J. Margot, M. Chaker, O. Pauna. *J. Appl. Phys*. **93**, 1907 (2003).
61. V. M. Donnelly, M. V. Malyshev. *Appl. Phys. Lett.* **77**, 2467 (2000).
62. V. M. Donnelly. *J. Vac. Sci. Technol. A* **14**, 1076 (1996).
63. C. S. Corr, E. Despiau-Pujo, P. Chabert, W. G. Graham, F. G. Marro, D. B. Graves. *J. Phys. D: Appl. Phys.* **41**, 185202 (2008).
64. A. D. Richards, H. H. Sawin. *J. Appl. Phys*. **62**, 799 (1987).
65. M. Moisan, Z. Zakrzewski. *J. Phys D: Appl. Phys.* **24**, 1025 (1991).
66. L. Stafford, R. Khare, V. M. Donnelly, J. Margot, M. Moisan. *Appl. Phys. Lett.* **94**, 021503 (2009).
67. J. Margot-Chaker, M. Moisan, Z. Zakrzewski, V. M. Galude, G. Sauvé. *Radio Sci.* **23**, 1120 (1988).
68. V. M. Donnelly. *J. Phys. D: Appl. Phys.* **37**, R217 (2004).
69. E. A. Ogryzlo. *Can. J. Chem*. **39**, 2556 (1961).
70. S. Wickramanayaka, N. Hosokawa, Y. Hatanaka. *Jpn. J. Appl. Phys.* **30**, 2897 (1991).

© 2010, IUPAC